Thermo-spectral properties of plastic lasers.

Nathan J. Dawson[1], Michael Aviles[1], James H. Andrews[1], Michael Crescimanno[1], Joshua B. Petrus[1], Anthony Mazzocco[1], Kenneth D. Singer[2,3], Eric Baer[3], and Hyunmin Song[3]

[1]Dept. of Physics & Astronomy, Youngstown State University, Youngstown, Ohio 44555, USA
[2]Dept. of Physics, Case Western Reserve Univ., Cleveland, OH 44106, USA
[3]Macromolecular Science & Engineering, Case Western Reserve Univ., Cleveland, OH 44106, USA

ABSTRACT

We study the effects of temperature changes on the operating wavelength of all-polymer microresonator lasers, particularly on multilayered defect distributed feedback and distributed Bragg reflector lasers. The parameters that change the operating wavelength are discussed with comparisons between experiments and simulations.

Keywords: microcavity, laser, temperature, stability, polymer

1. INTRODUCTION

All-polymer coextruded microcavity lasers can be made of many different plastics and dyes, and in diverse, tailorable layerings.[1,2] These polymer lasers can be made at low-cost[3] and with broad tunability.[4–6] In this paper, we discuss the parameters that affect two types of all-polymer lasers; (1) a Distributed FeedBack (DFB) and (2) a Distributed Bragg Reflector (DBR) laser. DFB lasers are made of alternating layers of undoped and dye-doped polymers and folded to create a spectral defect in the center of the reflection band.[5] DBR lasers are made with a thick dye-doped polymer as the active gain medium between the cavity reflectors consisting of bilayers of refractive index mismatched polymers.[7–10] These are created by coextruding a multilayer polymer film and then binding these multilayer films onto each side of a single gain layer. Both laser types depend on similar geometric structures, where significant reflection occurs from alternating refractive index mismatched polymers that make a one-dimensional photonic crystal (PhC).

In a temperature controlled environment, dye-doped polymer lasers that are constructed of PhCs can be temperature tuned to a desired wavelength. Particular designs and combinations of plastics in the PhCs can lead to a wide range of temperature coefficients of the lasing wavelengths, including very small temperature coefficients. Here, we discuss experiments on a defect DFB laser and two types of DBR lasers, where the structures are shown in Fig. 1. These microcavity lasers have a rhodamine 6g (R6G) doped gain medium and have previously been shown to operate at a range of wavelengths between 555-650 nm for the defect DFB lasers[11] and 565-615 nm for the elastomer DBR lasers.[4] We also give modeling results that show how transfer matrix methods can be used to determine the stability.

Figure 1. The structure of a DBR laser and defect DFB laser.

Further author information: (Send correspondence to N. J. D)
N. J. D.: E-mail: dawsphys@hotmail.com, Telephone: 1 216 368 4023

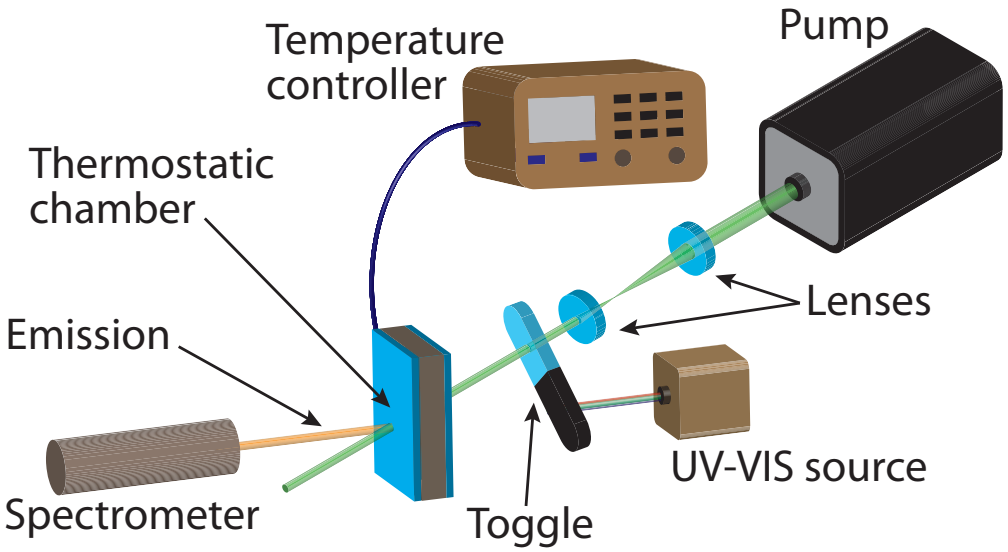

Figure 2. A diagram of the experimental setup. The temperature is increased inside a thermostatic chamber while the transmittance and laser emission spectra are recorded.

2. MATERIALS AND EXPERIMENTS

The all-polymer DFB laser is fabricated by the melt-process co-extrusion method.[1] This multilayer laser film is initially extruded with 32 bilayers (64 layers), and two (much thicker) protective low density polyethylene (LDPE) skin layers. These skin layers are removed post-processing. Each bilayer is made from a fluoroelastomer terpolymer layer of vinylidene fluoride, hexafluoropropylene, and tetrafluoroethylene (Dyneon THV 220G, refractive index=1.37) and an R6G dye-doped blended polymer layer of 75 wt% polystyrene and 25 wt% acrylonitrile (SAN25, refractive index=1.57). The bilayers have an average periodicity of 200 nm with an ∼18% layer-to-layer thickness variation, and a 1% nominal concentration by weight of R6G in the SAN25 layer.[1,10] In order to decrease the threshold and increase the lasing slope efficiency, the DFB laser film is folded in post-process to create a defect DFB laser.[5]

The all-polymer DBR lasers were also fabricated by the melt-process co-extrusion method.[1] The first type of DBR laser consists of multilayers of 64 bilayers (128 layers) and two R6G dye-doped skin layers. Each bilayer is made from a layer of ethylene-octene (EO) (Dow Engage 8842, refractive index=1.48) and a layer of THV. The skin layer is the gain medium consisting of an ethylene terpolymer composed of 40 wt% acrylic ester and glycidyl methacrylate (Lotador 8900) doped with 1 wt% R6G, with thickness ∼15 μm. The bilayers have an average periodicity of 220 nm with a ∼25% layer-to-layer thickness variation.[4] This DBR laser was made by removing a skin layer and folding on the other side to create an elastomer DBR laser with a ∼30 μm gain medium sandwiched between two 128-layer elastomeric multilayer reflectors. The second DBR laser was made by first placing a stand-alone Lotador skin layer on four stacked 32-layer polymer multilayer films, where the multilayer films are made of alternating layers of polystyrene (PS, refractive index=1.59) and poly(methyl methacrylate) (PMMA, refractive index=1.49). Then, the stacked films are folded to create a ∼30 μm dye-doped Lotador medium sandwiched between two 128-layer polymer multilayer reflectors. An electro-static force held the individual components together.

The multilayer laser films are placed in an insulated thermostatic chamber with transparent windows to transmit the pump and probe beams as shown in Figure 2. The lasers were pumped by a 7 ns pulsed 532 nm coherent laser source from a frequency doubled YAG laser, which coincides with the absorption band of R6G. The lasing wavelengths and transmission of the multilayer laser films were recorded by an Ocean Optics USB 4000. A 100 Ω ceramic resistor is located in the thermostatic chamber and in thermal contact with the laser films. The temperature inside the thermostatic chamber is increased at a slow rate to reduce temperature gradients between the laser film and the temperature probe. A K-type thermocouple was placed less than 2 mm from the lasing region. The defect DFB laser films are free standing in the thermostatic chamber. Because the DBR laser

films required post-process formation, these laser films were pinned to a glass coverslip prior to being placed in the thermostatic chamber. Note that the thermal expansivity of glass is much smaller than the plastics, so little translational motion occurs in the direction perpendicular to the dimension of the PhC for the DBR laser experiments.

Additional experiments were performed to characterize the thermal properties of the constituent materials. Both the volumetric thermal expansion coefficients and thermo-optic coefficients were estimated for monoliths of the defect DFB laser materials. The volumetric thermal expansion coefficient of THV was estimated by pinning two thin films between two mirrored substrates. The films acted as thermally tunable spacers in a Fabry-Perot interferometer, where the transmitted intensity from a 632.8 nm HeNe laser was measured to find the expansion in the direction normal to the surface of the mirrored substrates. Additionally, we embossed some monoliths with a diffraction grating and measured the change in the angle of diffraction as a function of temperature. The temperature dependence of the refractive index in monoliths of both materials was measured by a Horiba Uvisel DUV-NIR spectroscopic ellipsometer. Thin monoliths were spin-coated on silicon wafers and the measurements were performed with a probe beam at 70° from the direction normal to the substrate. These values were then used as starting parameters for nonlinear least-squares fitting of the defect DFB transmission spectra described in Section 5.

3. RESULTS

3.1 DFB material characterization

Monoliths of THV pinned between two mirrored substrates were found to have a linear coefficient of thermal expansion of $(5.5 \pm 1.0) \times 10^{-4}/\,^{\circ}\mathrm{C}$. Although the THV was pinned to a substrate, this data may be lower than the volumetric coefficient of thermal expansion. This may be due to the glass expanding with increasing temperature, and because THV is a soft elastomeric material that loses stiffness when heated, where the pressure between the two substrates may reduce the overall expansivity of THV.[12] We were unable to obtain a reliable linear thermal expansion coefficient for SAN25 using the same experiment. This is attributed to the small thermal expansion coefficient of SAN25 that made the fringe shifts unresolvable for thin films. The literature gives a value of $\sim 6.6 \times 10^{-5}/\,^{\circ}\mathrm{C}$ for the linear coefficient of thermal expansion of SAN25.[13]

We performed temperature dependent ellipsometry measurements to characterize the thermo-optical coefficients, dn/dT, of THV and SAN25, where n is the refractive index and T is the temperature. The thermo-optic coefficient of SAN25 was estimated to be $(1.1 \pm 0.3) \times 10^{-4}/\,^{\circ}\mathrm{C}$ while the thermo-optic coefficient of THV was estimated to be $(2.5 \pm 0.6) \times 10^{-4}/\,^{\circ}\mathrm{C}$. Alterations in the apparatus due to temperature fluctuations and difficulties in the nonlinear fitting of models with large numbers of parameters led to large uncertainties. Thus, in addition to modeling alternative systems in Section 5, we also attempt to reduce these uncertainties through nonlinear least squares fitting of the transmission spectra.

3.2 Defect DFB lasers

The transmission and emission spectra are shown in Fig. 3(a) for a set of experimental data taken from a defect DFB laser folded onto the side that is bounded by a layer of THV. This process created the defect DFB laser with a center defect layer of undoped THV. The corresponding movement of the peak lasing wavelength is shown in Fig. 3(c). The emission wavelength, λ_e, at room temperature was measured to be 603 nm, with a thermo-emission wavelength coefficient, $(1/\lambda_e)\, d\lambda_e/dT$, of $(2.33 \pm 0.17) \times 10^{-4}/\,^{\circ}\mathrm{C}$.

When we fold the multilayer film onto the side of a film bounded by a layer of SAN25, a defect DFB laser is created with a center defect layer of SAN25. The defect spectrally shifted a smaller amount per °C than the defect DFB laser that has a center THV double layer. This difference is observed directly by the transmission spectra shown in Fig. 3(b), where $\lambda_e = 598$ nm and $(1/\lambda_e)\, d\lambda_e/dT = (1.68 \pm 0.17) \times 10^{-4}/\,^{\circ}\mathrm{C}$. The peak emission wavelength as a function of temperature is shown in Fig. 3(d) from the same laser with transmission spectra shown in Fig. 3(b). The defect locations for lasers with a doubled SAN25 layer were found near the short wavelength edge of the reflection band, which is in contrast to the spectra observed in the THV doubled defect DFB lasers. The initial defect locations imply that the optical thickness of the center SAN25 layer in the defect DFB laser (folded on the SAN25 side) is less than twice the average optical thickness of the constituent layers,

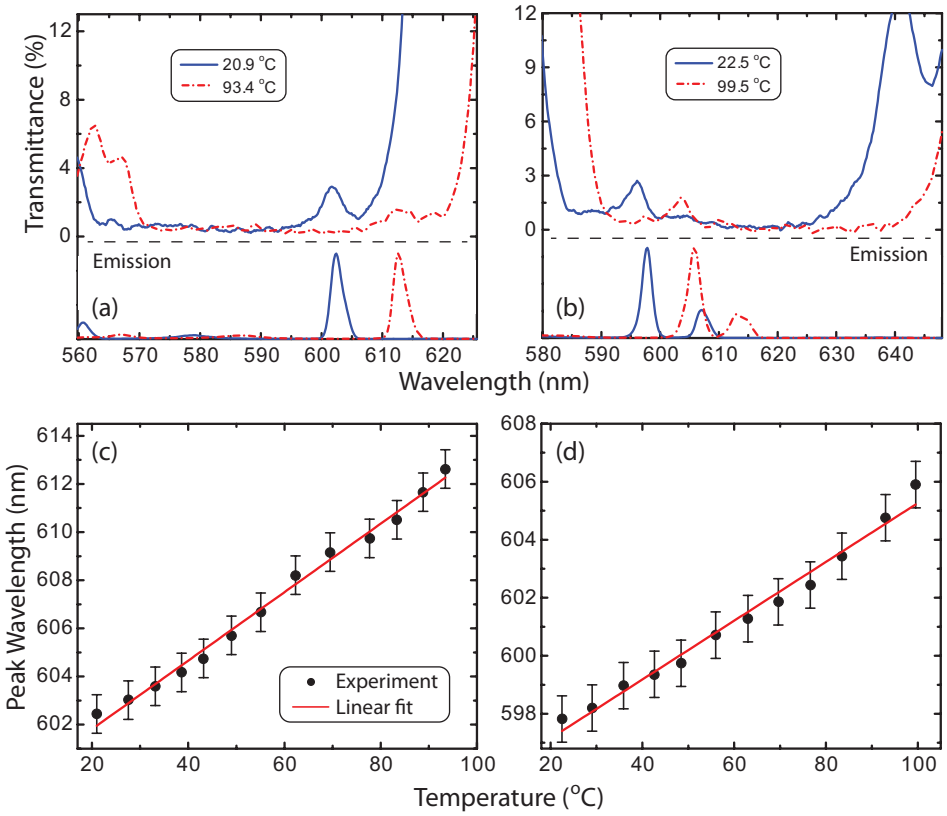

Figure 3. Transmission and emission spectra of defect DFB laser films folded on (a) undoped THV and (b) dye-doped SAN25. The peak lasing wavelength as a function of temperature for defect DFB lasers folded on (c) THV and (d) SAN25. The solid lines are linear fits to the experimental data.

while the optical thickness of the center THV layer (folded on the THV side) is greater than twice the average optical thickness of the constituent layers.

3.3 DBR material characterization

THV is a component of a Bragg reflector in one of our DBR lasers. The characterization of THV has already been described in Section 3.1. The 'grating method' was used to characterize the thermal expansion coefficient of PS and EO. Here, we emboss a diffraction grating on a monolith at elevated temperatures and then cool the sample to room temperature. Then we measure the change in the angle of the diffracted beam as we reheat the monolith. The measurement of the linear coefficient of thermal expansion for PS, $(7.3 \pm 1.3) \times 10^{-5}/\,^{\circ}\mathrm{C}$, was in good agreement with the literature value in Ref. 13. The linear coefficient of thermal expansion for EO was found in the same fashion, where we measured a value of $(5.1 \pm 2.0) \times 10^{-4}/\,^{\circ}\mathrm{C}$. The linear coefficient of thermal expansion for PMMA has been well characterized and we confirm the literature value of $\sim 6.5 \times 10^{-5}/\,^{\circ}\mathrm{C}$.[14]

Additional temperature dependent ellipsometry measurements were performed to characterize the thermo-optical coefficients of PMMA and EO. For PMMA, we found a value of $(-1.4 \pm 0.1) \times 10^{-4}/\,^{\circ}\mathrm{C}$, which is close to the literature value given in Ref. 15. The thermo-optical coefficient for EO was measured to be $(-3.6 \pm 0.5) \times 10^{-4}/\,^{\circ}\mathrm{C}$. A value of $(-1.4 \pm 0.1) \times 10^{-4}/\,^{\circ}\mathrm{C}$ is given in Ref. 16 for PS.

3.4 DBR lasers

The first of the two DBR lasers studied had two 128-layer reflectors made from alternating layers of THV and EO enveloping a $\sim 30\,\mu$m layer of Lotador, all of which are elastomeric materials. The thermo-emission wavelength coefficient was measure to be $(6.0 \pm 0.5) \times 10^{-4}/\,^{\circ}\mathrm{C}$ beginning at a wavelength of 601 nm at room temperature.

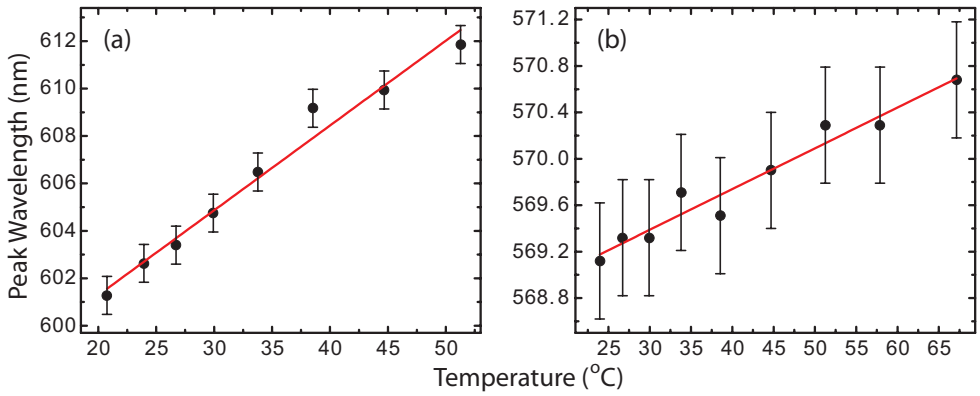

Figure 4. The peak lasing wavelength as a function of temperature for two DBR lasers made by enveloping an R6G-doped Lotador cavity by 128-layer films of alternating (a) THV/EO and (b) PS/PMMA. The lines in both graphs are the linear fits to the experimental data.

The second DBR laser employed a set of reflectors made from alternating layers of PS and PMMA to enclose a dye-doped Lotador gain medium. This laser had a thermo-emission wavelength coefficient of $(6.1 \pm 2.9) \times 10^{-5}/\,^{\circ}\mathrm{C}$ with the peak lasing wavelength at room temperature of 569 nm. Thus, using the same gain cavity and only changing the materials used in the reflectors, we were able to reduce the temperature sensitivity by an order of magnitude, as shown in Fig. 4.

4. DISCUSSION OF EXPERIMENTS

4.1 Defect DFB lasers

The physical parameters contributing to a thermo-emission wavelength coefficient are the gain envelope shift and geometry of the passive optical components. In multilayer laser films where the gain envelope is broad, the latter dominates and we now interpret the relevant laboratory measurements on these multilayer structures and their constituent plastics. In defect DFB laser films, the THV polymer has a large coefficient of thermal expansion as compared to the SAN25 blend. The expansion along the PhC dimension causes the spectral features of the PhC to shift toward longer wavelengths. Contrary to this, the multilayer constituents have a negative thermo-optic coefficient, and thus, reduce the naive thermal expansion induced spectral shift with temperature. Because the reflection band depends on the average *optical thickness* of all layers, and the preferred lasing wavelength is influenced by the spectral features within the reflection band, the peak emission wavelength will shift via changes in both the thickness and changes in the refractive indices.

In addition to the movement of the entire reflection band, the shift of spectral features per °C inside the reflection band is different from the shift per °C at the edges of the reflection band for many choices of bilayer materials and layer thickness distributions. In fact, the short- and long-wavelength reflection band edges each spectrally shift to longer wavelengths at different rates as the temperature is increased for the defect DFB lasers consisting of THV/SAN25 bilayers (note that the overall spectral width of the reflection band increases with temperature). Furthermore, the initial spectral location of the defect in the reflection band depends on the folded layer's (defect center layer's) optical thickness as compared to the average optical thickness of all other layers in the stack.[5, 17, 18] Also, the choice of the material used as the center defect layer affects the rate of change of the center defect layer's optical thickness relative to the rate of change in the optical thickness of the average layer for systems with bilayers composed of two separate materials with mismatched thermal properties. Therefore, the thermo-emission wavelength coefficient in defect DFB lasers depends on the shift per °C of the reflection band, the initial spectral location of the defect with respect to the band edges, and which bilayer material is used for the center defect layer.

The gain profile moved in a similar way for R6G dye-doped SAN25, where peak ASE shift of R6G-doped SAN25 as a function of temperature is 0.11 nm/ °C. Although the temperature dependence is similar to that of locations with the reflection band, the thermo-emission wavelength coefficients are distinctly different between

the two defect DFB laser configurations used in the experiment, confirming the dominance of the resonator structure over the gain envelope.

4.2 DBR lasers

The reflection band of the PS/PMMA multilayer reflectors is more thermally stable than the EO/THV reflectors, which we observed as an the order of magnitude difference in the thermo-emission wavelength coefficient. Again, we found that the optical properties of the resonators are the dominant influence with respect to the emission wavelength in comparison to thermal effects with the gain envelope. The movement of the gain profile as a function of temperature differs greatly from the movement of peak emission wavelength as a function of temperature, where the peak ASE shift of R6G-doped lotador as a function of temperature is 0.20 nm/ °C. Thus, we observe that the optical dispersion of the laser cavity has a greater influence on the emission wavelengths during operation than the gain profile, a point also made by Chua *et al.*[19]

Both of the DBR lasers studied have an R6G dye-doped Lotador gain medium. Lotador was found to undergo a volume reduction when the temperature was increased while all materials used in the Bragg reflectors volumetrically expand with temperature. Furthermore, the glass substrate expands slightly with temperature. The geometric configurations of the two types of DBR lasers are identical. Because the gain medium and substrate are the same in both types of laser experiments, the stiffness and magnitude of the volumetric thermal expansion coefficient of the materials used in the Bragg reflectors will dictate the degree to which their volumetric expansion is converted to linear expansion along the PhC dimension. Also, the thermo-emission wavelength coefficient is positive for both DBR lasers. Thus, the emission wavelength follows the reflectors. Our experiments show that altering the materials used in the Bragg reflectors drastically alters the thermo-emission wavelength coefficient. And so, a PS/PMMA multilayer DBR laser is more thermally stable with respect to the emission wavelength than a THV/EO multilayer DBR laser, where the latter may be referred to as a temperature tunable DBR laser.

5. NUMERICAL SIMULATIONS

5.1 DFB lasers

To more fully comprehend the relationship between the laser output wavelength and the temperature dependence of the optical path length of the layers in a PhC microcavity laser, we first study the THV/SAN25 defect DFB laser using transfer matrix theory.[20] The defect DFB laser is easier to model than the DBR laser due to the single defect mode in the former. The defect's position in the reflection band is a function of the phase accumulation, where high-Q microcavity lasing occurs. Thus, we can determine the peak output wavelength of the DFB laser as a function of temperature simply by tracking the defect in the transmission spectrum as a function of temperature.

5.1.1 Spectral fits

The volumetric expansion of THV is much larger than that of SAN25 such that the THV layers are pinned to the SAN25 layers, and therefore most of the thermal expansion in the THV layer is along the dimension of the PhC. Because the elastic modulus of SAN25 is much greater than that of THV, we will assume that the pull from the THV layers on the SAN25 layers causes a negligible deformation. Thus, we assume that the SAN25 layers increase their thickness by a linear strain that is 1/3 of the volumetric thermal expansion, while the THV layers that are pinned to the SAN25 layers change their thickness by a linear strain that is approximately equal to the volumetric thermal expansion. This is consistent with findings that thin films pinned on substrates primarily expand in the direction normal to the interface.[22]

The layer-to-layer thickness variations cause band edge deformations that alter the band edge shift as a function of temperature. By averaging several experimental runs of folded 64-layer THV/SAN25 laser films, we found that the short wavelength band edge shifts as $(1/\lambda_s)\, d\lambda_s/dT = 1.51 \times 10^{-4} \pm 1.6 \times 10^{-5}\,/\,^{\circ}\mathrm{C}$, and the long wavelength band edge shifts such that $(1/\lambda_l)\, d\lambda_l/dT = 2.35 \times 10^{-4} \pm 2.5 \times 10^{-5}\,/\,^{\circ}\mathrm{C}$, where λ_s denotes the short-wavelength band edge and λ_l denotes the long-wavelength band edge.

The spectral features measured in the simulations are produced by assuming a system of perfect layers with a center layer of variable thickness. A nonlinear least squares fitting routine based on Newton's method is used

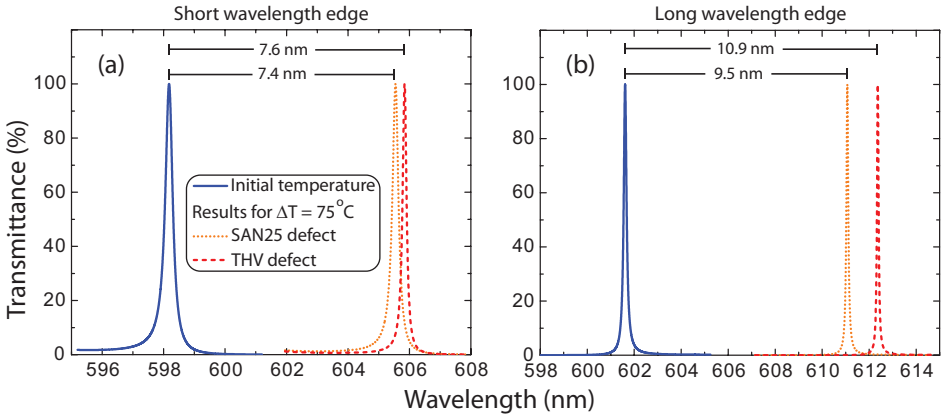

Figure 5. Simulations of the defect spectral location when the defect is positioned near the (a) short and (b) long wavelength edge of the reflection band.

to compare the optical parameters obtained from transfer matrix method simulations with those obtained by ellipsometry and interferometry measurements. The optical parameters obtained in the simulations are in good agreement with the literature and the independent monolith measurements done by our group. The thermo-optic coefficient for THV is in good agreement with that found in the characterization experiments, but the linear thermal expansion coefficient is slightly larger than the value obtained from independent monolith measurements. We attribute this larger value to a systematic error that was introduced via a constant pressure on the THV film from the apparatus, where the thermal expansion coefficient of THV blends have been shown to decrease with increased pressure.[12] The thermo-optic coefficient of styrene acrylonitrile given by Ref.[23] is also within the bounds of our measurements.

5.1.2 Simulations

The motion of the reflection band defect location in defect DFB laser films as a function of increasing temperature was measured to be up to 1.7 times greater in defect lasers folded on the THV side as compared to lasers folded on the SAN25 side. Systematic layer thickness deviations in the available laser films, however, did not produce evenly distributed defect locations across the reflection band. The defects from THV-folded systems appear near the long-wavelength edge of the reflection band, while the defects from SAN25-folded systems are closer to the short-wavelength edge of the reflection band. Using the parameters obtained from the spectral fits and monolith measurements we simulate systems that may have defects at different locations in the reflection band. Similar to the fitting routines, we assume perfect layer thicknesses except for the center layer, and choosing its thickness to position the defect at a particular location of the reflection band. Assuming that the defect location as a function of temperature is the laser emission wavelength, we find that $(1/\lambda_e)\, d\lambda_e/dT|^{\mathrm{SAN25}}_{\mathrm{short}} \approx 1.65\times10^{-4}/\,^{\circ}\mathrm{C}$ and $(1/\lambda_e)\, d\lambda_e/dT|^{\mathrm{THV}}_{\mathrm{long}} \approx 2.42\times10^{-4}/\,^{\circ}\mathrm{C}$, where the subscripts "short" and "long" describe the region of the defect's location with respect to the short or long wavelength edge of the reflection band, and the superscripts "SAN25" and "THV" denote the material used as the center defect layer. If we choose the center layer to be opposite that of the experiment but assume similar spectral characteristics of that seen in the experiment for the original layer configuration, then we predict $(1/\lambda_e)\, d\lambda_e/dT|^{\mathrm{SAN25}}_{\mathrm{long}} \approx 2.09\times10^{-4}/\,^{\circ}\mathrm{C}$ and $(1/\lambda_e)\, d\lambda_e/dT|^{\mathrm{THV}}_{\mathrm{short}} \approx 1.69\times10^{-4}/\,^{\circ}\mathrm{C}$. Thus using the mean parameter values, we find that by changing the material used as the center defect layer, defects occurring near the experimental location found near the short-wavelength band edge showed a difference of approximately $0.003\,\mathrm{nm}/\,^{\circ}\mathrm{C}$ between the two thermo-emission wavelength coefficients. Defects occurring near the experimental location found near the long-wavelength band edge, however, had a greater difference of approximately $0.022\,\mathrm{nm}/\,^{\circ}\mathrm{C}$. These numerical simulations are shown in Fig. 5.

The results from transfer matrix theory show a large difference in defect movement between the THV centered defect layer and the SAN25 centered defect layer. The large amount of material in the center layer for the defect located near the long wavelength band edge (greater than twice the thickness of a standard layer for folded systems to create a defect at that spectral location) allows for materials with large coefficients of thermal expansion, such as THV, to dominate at the center layer. In contrast, SAN25 has a much lower coefficient of thermal expansion

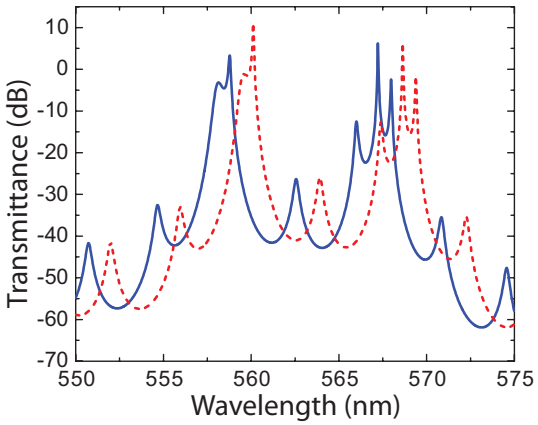

Figure 6. Simulations of the transmittance using the three slab model with gain in the center slab. The solid line is at room temperature and the dashed line is at an elevated temperature.

and the corresponding defect moves a shorter distance with increasing temperature. Also, defects that appear near the short wavelength side of the reflection band have center layer thicknesses that are less than twice the average layer thickness, and they are more comparable to the average layer thickness. Therefore, we see smaller differences in defect motion between folded lasers having a center defect layer with less than twice the average layer thickness.

5.2 DBR lasers

A simplified model is used to study the temperature coefficient of the DBR lasers' emission. Consider a three slab laser; the center slab is the gain layer and the two enveloping slabs, with large indices of refraction, are the mirrors. A flat gain is assumed in the center layer. The highest output transmittance corresponds to the spectral location of the first lasing mode. The high index slabs change thickness with temperature. As illustrated in Fig. 6, the gain spectrally shifts to different wavelengths as the temperature is increased (corresponding to a change in thickness of the reflective layers). The scalloping transmission modes are the cavity modes, but they pile up and brighten due to dispersion in the slab reflectors. This mode 'pile-up' is associated with a greater density of states (in one dimension this is the same as a low group velocity) and results in the brightening. Thus, the lasing wavelength is locked to the dispersion features of the mirrors and not to that of the of the gain cavity. This means that for DBR lasers with dielectric mirrors, the thermo-emission wavelength coefficient is dominated by the temperature coefficients of the mirrors and not the cavity.

6. CONCLUSIONS

The temperature tunability and stability of all-polymer DBR and defect DFB laser films have been studied for select materials. We found that for DBR laser films, the cavities with PS/PMMA reflectors are temperature stable. The output wavelength for the cavities with EO/THV reflectors, however, dramatically shifts to longer wavelengths as the temperature increases. Thus, by simply changing materials, an all-polymer laser can be made temperature stable or temperature tunable.

The defect DFB lasers were characterized and the peak laser wavelength was shown to depend on the defect location within the reflection band. Models of both types of lasers show that the thermal expansion coefficient and thermo-optic coefficient play a larger part in peak wavelength selection than the gain medium. The defect DFB was further studied to show, although to a lesser degree, that the location of the single cavity mode can also affect the temperature tunability of the operating wavelength.

This study gives insights into the thermal tunability and stability of plastic lasers. The sizable amount of materials with a large distribution of parameters associated with the thermo-emission wavelength coefficient give all-polymer lasers an advantage to a broad range of applications. The thermal stability that some of these materials exhibit will be useful for applications requiring stability in the operating wavelength that are placed in environments with large local temperature variations.

REFERENCES

[1] T. Kazmierczak, H. Song, A. Hiltner, and E. Baer, "Polymeric one-dimensional photonic crystals by continuous coextrusion," *Macromol. Rapid Commun.* **28**(23), 2010–2016 (2007).

[2] H. Song, *Melt-processable polymeric photonic crystals and their applications as nano-layered laser films*, PhD thesis, Case Western Reserve University (2012).

[3] H. Song, K. D. Singer, J. Lott, Y. Wu, J. Zhou, J. H. Andrews, E. Baer, A. Hiltner, and C. Weder, "Continuous melt processing of all-polymer distributed feedback lasers," *J. Mater. Chem.* **19**, 7520–7524 (2009).

[4] G. Mao, J. H. Andrews, M. Crescimanno, K. D. Singer, E. Baer, A. Hiltner, H. Song, and B. Shakya, "Co-extruded mechanically tunable multilayer elastomer laser," *Opt. Mater. Express* **1**(1), 108–114 (2010).

[5] J. H. Andrews, M. Crescimanno, N. J. Dawson, G. Mao, J. B. Petrus, K. D. Singer, E. Baer, and H. Song, "Folding flexible co-extruded all-polymer multilayer distributed feedback films to control lasing," *Opt. Express* **20**(14), 15580–15588 (2012).

[6] J. H. Andrews, M. Aviles, M. Crescimanno, N. J. Dawson, A. Mazzocco, J. B. Petrus, K. D. Singer, E. Baer, and H. Song, "Thermo-spectral study of all-polymer multilayer lasers," *Opt. Mater. Express* **3**(8), 1152–1160 (2013).

[7] K. D. Singer, T. Kazmierczak, J. Lott, H. Song, Y. Wu, J. H. Andrews, E. Baer, A. Hiltner, and C. Weder, "Melt-processed all-polymer distributed Bragg reflector laser," *Opt. Express* **16**(14), 10358–10363 (2008).

[8] K. D. Singer, T. Kazmierczak, J. Lott, H. Song, Y. Wu, J. H. Andrews, E. Baer, A. Hiltner, and C. Weder, "Toward Roll-to-Roll Production of Polymer Microresonator Lasers," *Opt. Photonics News* **19**(12), 28–28 (2008).

[9] J. Lott, H. Song, Y. Wu, J. Zhou, E. Baer, A. Hiltner, C. Weder, and K. D. Singer, [*Coextruded Multilayer All-Polymer Dye Lasers*], ch. 13, 171–184 (2010).

[10] J. Zhou, K. D. Singer, J. Lott, H. Song, Y. Wu, J. H. Andrews, E. Baer, A. Hiltner, and C. Weder, "All-Polymer Distributed Feedback and Distributed Bragg-Reflector Lasers Produced by Roll-to-roll Layer-Multiplying Co-Extrusion," *Nonlinear Opt. Quant. Opt* **41**(1), 59–71 (2010).

[11] N. Dawson, K. D. Singer, J. H. Andrews, M. Crescimanno, G, Mao, J. B. Petrus, H. Song, and E. Baer, "Post-Process Tunability of Folded One-Dimensional All-Polymer Photonic Crystal Microcavity Lasers," *Nonlin. Opt. Quant. Opt.* **45**(1-2), 101–111 (2012).

[12] D. M. Dattelbaum, S. A. Sheffield, D. Stahl, M. Weinberg, and C. Neel, "Equation of state and high pressure properties of a fluorinated terpolymer: THV 500," *J. Appl. Phys.* **104**(11), 113525 (2008).

[13] J. F. Shackelford and W. Alexander, [*Materials Science and Engineering Handbook*], CRC Press LLC, Boca Raton, 3rd ed. (2001).

[14] R. Simha and R. F. Boyer, "On a General Relation Involving the Glass Temperature and Coefficients of Expansion of Polymers," *J. Chem. Phys.* **37**(5), 1003–1007 (1962).

[15] J. M. Cariou, J. Dugas, L. Martin, and P. Michel, "Refractive-index variations with temperature of PMMA and polycarbonate," *Appl. Opt.* **25**(3), 334–336 (1986).

[16] S. Krause, and Z. H. Lu, "Refractive index-temperature measurements on anionically polymerized polystyrene," *J. Polym. Sci.: Polym. Phys. Ed.* **19**(12), 1925–1928 (1981).

[17] E. Yablonovitch, "Inhibited spontaneous emission in solid-state physics and electronics," *Phys. Rev. Lett.* **58**(20), 2059–2062 (1987).

[18] E. Yablonovitch, T. J. Gmitter, R. D. Meade, A. M. Rappe, K. D. Brommer, and J. D. Joannopoulos, "Donor and Acceptor Modes in Photonic Band Structure," *Phys. Rev. Lett.* **67**(24), 3380–3383 (1991).

[19] S. L. Chua, Y. Chong, A. D. Stone, M. Soljačić, and J. Bravo-Abad, "Low-threshold lasing action in photonic crystal slabs enabled by Fano resonances," *Opt. Express* **19**(2), 1539–1562 (2011).

[20] P. Yeh, [*Optical Waves in Layered Media*], John Wiley & Sons, Inc., Hoboken (2005).

[21] J. Yoon, W. Lee, J. M. Caruge, M. Bawendi, E. L. Thomas, S. Kooi, and P. N. Prasad, "Defect-mode mirrorless lasing in dye-doped organic/inorganic hybrid one-dimensional photonic crystal," *Appl. Phys. Lett.* **88**(9), 091102 (2006).

[22] D. J. Pochan, E. K. Lin, S. K. Satija, and W. Wu, "Thermal Expansion of Supported Thin Polymer Films: A Direct Comparison of Free Surface vs Total Confinement," *Macromolecules* **34**(9), 3041–3045 (2001).

[23] J. D. Lytle, "Polymer optics," in [*Handbook of Optics*], Bass, M., ed., McGraw-Hill, Inc., New York, 2nd ed. (1995).